NEUROIMAGE **6,** 245–258 (1997)
ARTICLE NO. NI970301

Visualization-Based Mapping of Language Function in the Brain

B. Modayur,* J. Prothero,* G. Ojemann,† K. Maravilla,‡ and J. Brinkley*

**Structural Informatics Group, Department of Biological Structure, †Department of Neurosurgery, and ‡Department of Radiology, University of Washington, Seattle, Washington 98195*

Received April 17, 1997

Cortical language maps, obtained through intraoperative electrical stimulation studies, provide a rich source of information for research on language organization. Previous studies have shown interesting correlations between the distribution of essential language sites and such behavioral indicators as verbal IQ and have provided suggestive evidence for regarding human language cortex as an organization of multiple distributed systems. Noninvasive studies using ECoG, PET, and functional MR lend support to this model; however, there as yet are no studies that integrate these two forms of information. In this paper we describe a method for mapping the stimulation data onto a 3-D MRI-based neuroanatomic model of the individual patient. The mapping is done by comparing an intraoperative photograph of the exposed cortical surface with a computer-based MR visualization of the surface, interactively indicating corresponding stimulation sites, and recording 3-D MR machine coordinates of the indicated sites. Repeatability studies were performed to validate the accuracy of the mapping technique. Six observers—a neurosurgeon, a radiologist, and four computer scientists, independently mapped 218 stimulation sites from 12 patients. The mean distance of a mapping from the mean location of each site was 2.07 mm, with a standard deviation of 1.5 mm, or within 5.07 mm with 95% confidence. Since the surgical sites are accurate within approximately 1 cm, these results show that the visualization-based approach is accurate within the limits of the stimulation maps. When incorporated within the kind of information system envisioned by the Human Brain Project, this anatomically based method will not only provide a key link between noninvasive and invasive approaches to understanding language organization, but will also provide the basis for studying the relationship between language function and anatomical variability.

INTRODUCTION

Cortical language maps obtained through intraoperative electrical stimulation studies provide a rich source of information for research on language organization. Through intraoperative stimulation studies, cortical sites essential for language function can be identified. Non-computer-based studies have shown interesting correlations between the distribution of essential language sites and such behavioral indicators as verbal IQ (Ojemann *et al.*, 1989a). These empirical observations lead to interesting speculations about whether distribution of language, or any other function, can be related to variations in cortical anatomy and whether function can be predicted from anatomy alone. Further validation of this apparent relationship between function and anatomy could be made possible by the integration of stimulation data with data from other modalities such as fMRI, PET, SPECT, and ECoG.

The stimulation data also provide suggestive evidence for regarding human language cortex as an organization of multiple distributed systems (Haglund *et al.*, 1993; Ojemann *et al.*, 1989a; Ojemann, 1991), each involved in the processing of a distinct language function, with all the different systems acting in parallel. The distributed model has received additional support through the use of other techniques. ECoG recordings from electrodes placed on the exposed cortical surface show correlation with the essential naming sites during object naming in the absence of electrical stimulation (Ojemann *et al.*, 1989b). Optical imaging on a few patients shows changes near the essential sites that are absent in areas without essential sites, but the activation areas are larger (Haglund *et al.*, 1992). Use of other noninvasive techniques such as fMRI (Binder *et al.*, 1996, 1995) and PET (Petersen *et al.*, 1988; Demonet *et al.*, 1992) have also lent additional support to the distributed language model. PET and fMRI, however, reveal areas of activation as opposed to areas of inhibition revealed by stimulation studies.

Although many studies have described the integration of multiple imaging modalities (Levin *et al.*, 1989; Evans *et al.*, 1991), only one or two hint at the integration of electrical stimulation data with functional data obtained from noninvasive sources such as fMRI and PET (Herholz *et al.*, 1997). If surgical data can be

1053-8119/97 $25.00

integrated with noninvasive functional methods, and if the language areas as revealed by the two methods are found to be highly correlated, then it may be possible to altogether supplant intraoperative studies with the more convenient noninvasive methods.

Two approaches are possible for integrating these two kinds of data: (a) 3-D locators, and (b) 3-D reconstruction followed by visual mapping. The first approach involves using a 3-D locator device secured to the patient head, which the surgeon can use to locate language sites and record the 3-D location of the sites. The 3-D locator can be registered to the MR data of the patient through the use of surface markers on the patient head. This will enable correlation of stimulation data with noninvasive data obtained from sources such as MR and PET. However, changes in cortical morphology as a result of craniotomy complicate this registration process. In addition, the need to secure the locator device to the patient, and the potential inconvenience to the awake patient of such a device, makes this approach impractical when the locator is not otherwise needed during surgery.

The alternate approach, which we describe in this paper, is visual comparison between an MR-based 3-D cortical reconstruction and an intraoperative photograph (Fig. 1) of the exposed cranial surface. Mapping is then done by manually indicating on the visualized surface the location of stimulation sites visible on the photograph. Since visual comparison entails recognition of cortical structures by the mapper (human expert), this technique tolerates changes in morphology that occur during surgery. Also, since the visual comparison approach uses only the intraoperative photograph and the MR scans, it is possible to implement it with minimal change to the operation protocol and without inconveniencing the patient. In fact, the only change in the protocol is the acquisition of MR data prior to surgery.

The remainder of this paper describes our methods for generating the computer-based visualization and for mapping the stimulation sites onto the 3-D model. Repeatability results are then presented which show that this technique is accurate within the limits of the surgical sites.

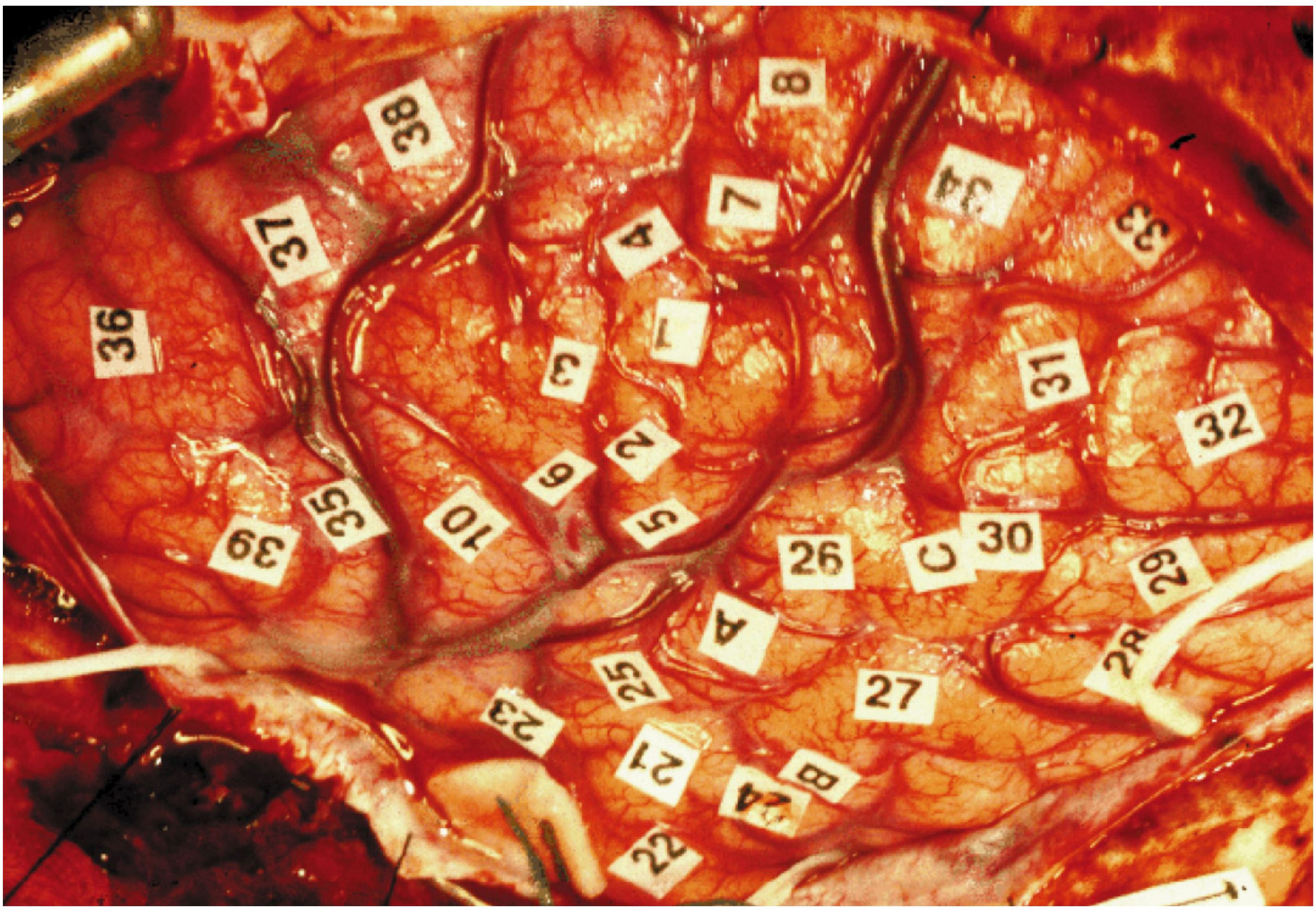

FIG. 1. Intraoperative photograph obtained after stimulation mapping. Sites that were included in the stimulation study are marked with numbered tags.

METHODS

The goal of the visualization and mapping procedure is to generate the location and extent of the stimulation mapping sites with respect to a uniform, 3-D patient coordinate system. The language sites of individual patients can then be combined with or related to other patient data in terms of a Talairach, surface-based, or other deformable coordinate system.

The language mapping process is carried out in the following order: (i) image acquisition, (ii) surgical stimulation, (iii) image enhancement, (iv) alignment, (v) cropping, (vi) cortical segmentation, (vii) surface visualization, and finally (viii) interactive mapping. The overall flow of data is shown in Fig. 2.

Our heterogeneous software environment consists of Advanced Visual Systems' (AVS), a commercial data visualization package, and Skandha4, an in-house graphics program (Brinkley and Prothero, 1997). Both these programs run on Silicon Graphics computers.

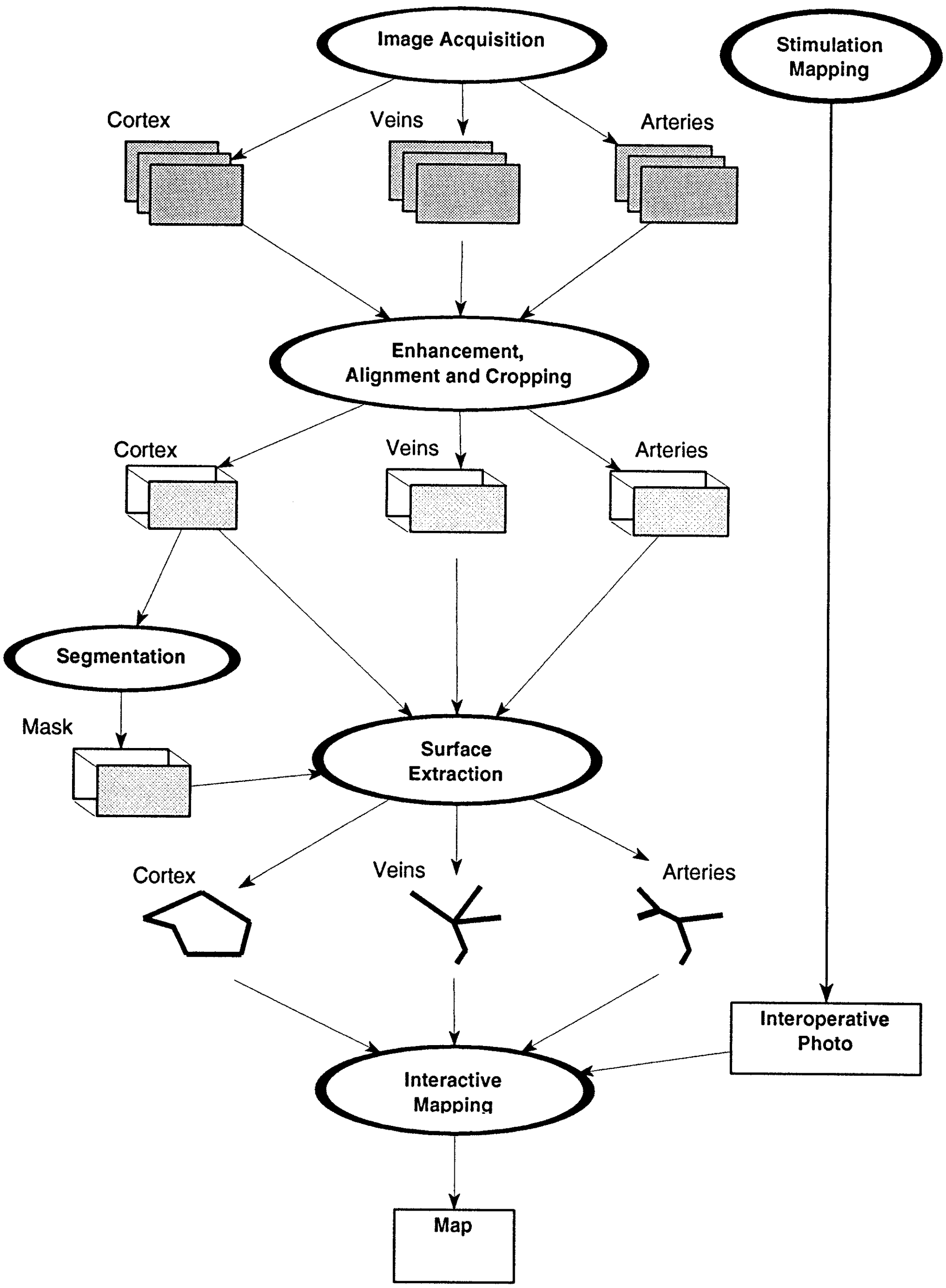

FIG. 2. Overall dataflow for visualization and mapping.

The alignment and interactive language mapping are carried out in Skandha4, while the rest of the stages are currently implemented in AVS. Later versions will be entirely implemented in Skandha4 because of its more efficient use of memory.

The following paragraphs describe the language mapping process in more detail.

Image Acquisition

Image acquisition is usually carried out the evening prior to surgery. All studies are performed on a whole body 1.5 Tesla MR scanner (SIGNA, General Electric Medical Systems, Milwaukee, WI). The patient's head is positioned in a specially designed, close fitting, birdcage-type RF head coil that provides an increase in signal-to-noise ratio of approximately 40% compared with the standard quadrature head coil (Hayes *et al.*, 1993), which roughly equates to a twofold increase in number of signal averages. Following a fast localizer to confirm patient position, a total of three sequences are obtained. The first sequence is a 3-D volume image of the entire brain from which the cortical anatomy is obtained. The other two are flow-sensitive studies that provide detailed maps of surface arteries and veins, respectively, which are used as landmarks for localizing the exposed cortical surface during neurosurgery.

3-D SPGR. This sequence is a three-dimensional (volume) gradient recalled echo with a radio frequency spoiler pulse. The imaging parameters are (29/5/1/45°) [TR/TE/NEX/flip angle], 22 cm FOV, 256 × 192 matrix, and 124 1.2 mm sagittal partitions. This yields a T1-weighted image of the entire brain which results in very detailed images of the ventricles, cisterns, surface anatomy of the sulci and gyri, together with excellent visualization of gray and white matter. The cortical data consists of 124 sagittal slices at 1.2-mm spacing.

2-D TOF MR Venogram. This sequence is a two-dimensional time-of-flight MR angiogram that utilizes a gradient recalled echo image optimized for flow related enhancement of the cortical veins, which appear bright on a dark background. The imaging parameters for this sequence are (45/9/1/60°), 22 cm FOV, 256 × 192 matrix, and 100 individual contiguous axial images of 1.5-mm thickness. This study is performed in a sequential mode in the axial plane. An inferior spatial presaturation pulse is parked at the skull base to suppress arterial inflow signal. The entire venous system of the brain is imaged with this technique.

3-D MOTSA MR arteriogram. This is a three-dimensional (volume) gradient recalled echo pulse sequence that is obtained using multiple overlapping thin slabs and a variable flip angle excitation pulse, to improve sensitivity for inflow of unsaturated arterial blood (RAMP Excitation, GE Medical Systems, Milwaukee, WI). This MRA study is performed in the axial plane at high resolution to visualize small arterial structures which appear bright on a dark background. Imaging parameters include 4 overlapping slabs of 16 partitions each (36/6.9/1/25°), flow compensation, 22 cm FOV, and 256 × 256 matrix. A superior saturation pulse is applied to suppress signal from venous flow. The study encompasses the major arteries at the base of the brain and extends up to the roof of the lateral ventricles. It is centered through the Sylvian fissure region to visualize small middle cerebral artery branches in this region. Arterial data consists of 64 axial slices at 0.9-mm spacing.

All datasets are acquired with a 22-cm field of view which is referenced to the magnet isocenter (an imaginary point in space within the center of the magnet which represents the intersection of the three orthogonal planes) to allow registration of the datasets for image postprocessing. The patient is immobilized using stiff sponges wedged between the head and the sides of the bird-cage head coil. Once the images have been acquired they are stored on a GE optical disk in the Radiology Department, then transferred over the network to Silicon Graphics computers in the Department of Biological Structure.

Stimulation Mapping

Since essential language sites are variable among patients, stimulation mapping is routinely performed in order to plan resections for the treatment of left temporal tumor or intractable epilepsy at the University of Washington (Ojemann *et al.*, 1989a). Surgery is usually performed the day following image acquisition. The stimulation studies are done for an object naming task, although other tasks are used on a subset of patients. After the initial craniotomy has been performed, an initial set of sites chosen for stimulation study is marked with numbered tags placed on the exposed cortical surface (Fig. 1). The awake patient is now shown slides of familiar objects, such as planes, boats, and trees, and is required to perform object naming. For every other slide, the neurosurgeon applies a small electric current (1.5 to 10 mA) to the selected numbered sites, for a total of approximately three stimulations per site. If the stimulation of a site leads to object naming errors at least two of three times, even though the patient can name the object correctly in the absence of any stimulation, the site is determined to be essential for language function. These sites are considered essential for language because: (a) resecting tissue close to such areas usually results in postoperative aphasia, (b) avoiding them by 1.5 to 2 cm avoids such language deficits, and (c) all aphasic syndromes include anomia (Ojemann *et al.*, 1989a). Prior to resection, a photograph is taken of the exposed cortex with the numbered tags denoting the stimulation sites

(Fig. 1). The photograph, together with a table recording which of the language sites have been found to be essential, comprise the surgical input to the mapping process.

Enhancement, Alignment, and Cropping

In order to generate a 3-D visualization to match the photograph, the MR datasets are processed using relatively standard image processing algorithms: enhancement, alignment, cropping, segmentation, and surface rendering.

Enhancement was required for the cortex (3-D SPGR) dataset on some of our earlier patients because the RF head coil produced a gradient artifact that interfered with segmentation. This artifact manifested itself as an intensity fall off across the volume data. The RF inhomogeneity present in these datasets can be modeled as a low frequency signal in contrast to the high frequency information present in the underlying anatomy. This intraslice intensity variation can be corrected using (a) phantom acquisition (Axel *et al.*, 1987), or retrospectively using (b) homomorphic filtering (Lim and Pfefferbaum, 1989; Axel *et al.*, 1987), or (c) interactive correction using surface fitting techniques (Dawant *et al.*, 1993). We found that a simple homomorphic filtering was sufficient to remove the gradient artifact. The intensity gradient for each image is modeled as a multiplicative, low-frequency noise factor. Thus, the observed signal is considered a product of the original signal with the noise factor: $M = A \times I$, where M is the observed image, A is the noise factor, and I is the signal image.

A 19-pixel-wide square kernel is used to convolve the observed image M to produce the low frequency image A. By taking the logarithm of the observed image M and subtracting the log of the low-frequency image A, the log of the original signal I can be obtained: $\log I = \log M - \log A$; $\log I$ is then exponentiated to get the final output image, in which the intensity fall off artifact has been removed.

Whether or not the inhomogeneity correction is needed, in the next stage the three datasets are *aligned* in 3-D. For the purposes of this study, it is assumed that patient motion between the three MR studies, which take approximately 50 min, is negligible. This assumption was made because these patients are generally cooperative and highly motivated individuals. Although the assumption is not strictly correct, the slight misregistration caused by patient movement between sequences is minimal. Since blood vessels are used only to identify and localize cortical structures for visual matching, it is not necessary that the alignment be exact.

Each exam series is acquired using similar image volume sizes (i.e., fields of view or FOV), but at a different orientation and spatial resolution. However, the MR machine keeps track of the relationship of each series to a fixed coordinate system in the center of the magnet and records this information in the image headers. Thus, to align the three volume datasets we extract, from the supplied header information, the slice thickness, slice spacing, voxel size, image matrix size, and position of each image volume with respect to the magnet coordinate system. The datasets then undergo a three-step process. First, the datasets are rotated in 90° increments until all three are in the same machine-space orientation. A minimum bounding box is then established with a grid of cubic voxels, and finally the data from the rotated volumes are resampled into the grid.

The resulting datasets are of identical dimensions in a $256 \times 256 \times 256$ voxel array, in which the i, j, and kth voxel in each dataset corresponds to the same physical location in MR-machine space, assuming there is no patient movement.

This alignment procedure is similar to that produced by the *ge2mni* perl script, written by Peter Neelin (Montreal Neurological Institute, 1996). Visual comparisons were made between alignments produced by both techniques in order to verify the correctness of the software.

The alignment procedure is followed by a *cropping* operation in order to reduce the size of the volume datasets for effective processing in AVS. This operation is necessary in AVS because of its inefficient use of memory. Although cropping does not affect the validity of the current results, it will not be needed when these methods are ported to a more efficient software environment.

Cropping is done using an AVS graphical user interface to cut off all but a slab near the left temporal surface, on all three aligned volumes. Cropping reduces the size of the datasets from over 100 megabytes to less than 10 megabytes, while still retaining enough information for satisfactory renderings. The cropped datasets are input to the segmentation module.

Cortical Segmentation

Segmentation of the cortex from the surrounding background is not necessary for strict visualization of the cortex through volume rendering methods. However, the goal of the mapping process is to determine the 3-D coordinates of points on the surface, thereby requiring that the surface be extracted from the image data. Common approaches to cortical segmentation include 3-D region growing and deformable models (MacDonald *et al.*, 1995). Since the surgical sites are not located within deep sulci it is not necessary at this stage to segment the detailed sulcal anatomy. Therefore, a simple 3-D region growing approach is sufficient. However, standard region growing algorithms often fail for cortical segmentation because of small connections between cortical regions and surrounding skull. For this reason we have developed an adaptive region grower, called *region grow,* that uses a cost function to determine when to add voxels to a growing region (Myers and Brinkley, 1995).

The basic idea behind *region grow* is that voxels belonging to the same tissue type and adjacent to each other will have fairly homogeneous grayscale properties. The algorithm thus attempts to find these initial or seed areas by looking for voxels whose neighborhood variance is below a user-specified threshold. Regions are then grown recursively from these seed voxels. As the regions begin to grow in size, the algorithm starts considering grayscale characteristics of the growing region as well as adjacency constraints of other voxels in the region. More formally, for a given voxel, v, whose 26-adjacent neighborhood, N, contains at least one voxel belonging to a growing region R, v will be included in R if $cost < 1$, where:

$$cost = \left(\frac{1}{T_R}\right)\frac{(I_v - \hat{x_R})^2}{\sigma_R^2}\, w + \frac{\sigma_N^2}{T_N}\,(1 - w),$$

where I_v = intensity of given voxel, v; T_R = threshold for region R; T_N = threshold for neighborhood N; $\hat{x_R}$ = intensity mean of voxels in R; σ_R^2 = intensity variance of voxels in R; σ_N^2 = intensity variance of voxels in neighborhood N; and w = a weighting factor.

The weighting factor, w, is determined by three user-specified parameters: a voxel counter $g_{\min}$, a second voxel counter g_{window}, and a percentage P_{grey}. Let n_R be the number of voxels in R, then the weight w is defined by,

$$w = \begin{cases} 0 & \text{if } n_R < g_{\min} \\ P_{\text{grey}}\left(\dfrac{n_R - g_{\min}}{g_{\text{window}}}\right) & \text{if } g_{\min} \le n_R \le g_{\min} + g_{\text{window}} \\ P_{\text{grey}} & \text{if } n_R > g_{\min} + g_{\text{window}} \end{cases}$$

This has the effect of causing regions to grow initially based only on local smoothness, since $w = 0$, but beyond $n_R > g_{\min}$, to consider progressively the voxel's greyscale intensity relative to R up to a fixed percentage, P_{grey}. That is, the cost will be high if a voxel's intensity is too different from that of R.

In addition to intensity similarity encoded in the cost value, adjacency criteria encode general shape knowledge. By adjacency constraints, voxel v will definitely be included in R if the number of adjacent voxels belonging to R exceeds a user-defined threshold (typically 16 to 18), even if the cost is greater than 1. Conversely, v will be excluded from R if the number of adjacent voxels belonging to R is less than the user-defined minimum (typically 2–4). While the minimum adjacency criteria prevents the expansion of regions along a single line of voxels, the maximum adjacency criteria prevents the exclusion of voxels that are otherwise surrounded by several voxels already in the growing region.

Region grow is applied to the anatomy (3-D SPGR) image dataset. The output is a labeled volume, where the label indicates the membership of a voxel in a segmented object. The segmented objects are viewed via a movable 2-D slice plane in AVS, and the object corresponding to the cortical tissue is selected by the user. The ROI mask thus derived is then postprocessed by 3-D morphological operators, to smooth the mask and to expand it so that we capture the superficial blood vessels in the surface extraction process.

Surface Extraction

The visualization module of the brain mapper produces a 3-D rendering of the cortical surface along with the associated superficial veins and arteries. Visualization methods for volume data can be broadly classified (Elvins, 1992) into (a) surface-fitting techniques that fit geometric primitives (usually planar) to volume data and render the primitives using conventional surface rendering algorithms, and (b) direct volume rendering methods that project voxels directly onto a 2-D image space without using any intermediate primitives. In earlier work the output of *region grow* was used to mask out the scalp in a volume rendering method (Myers and Brinkley, 1995). However, renderings generated by that method were not as detailed as those we have since obtained using surface-based approaches. Since in the long run we need the 3-D coordinates of points on the surface of the brain our current approach is to develop surface-based visualization methods.

The approach we take to extracting surfaces from volume data is to use *region grow* to produce a ROI mask, as in the volume visualization approach. The mask is used to exclude noncortical tissue from the volume data before running a generic isosurface algorithm (Lorensen and Cline, 1987) provided by AVS, called *isosurface,* to produce the cortical surface. The mask is also morphologically processed to generate a 3-D annular region that is applied to the arterial and venous data so that only surface vessels are extracted by the isosurface module.

The three generated surfaces are passed to the mapping program for surface visualization and interactive mapping.

Interactive Mapping

Language site mapping is done using the Skandha4 package. The three surface models produced by AVS (one each for cortex, veins, and arteries), the corresponding intraoperative photograph, and the original MR volume data, are loaded into the language mapping module. Skandha4 controls are used to manipulate color, lighting, surface properties, and viewpoint of the rendered models. The interface is shown in the screen dump of Fig. 3.

The language site mapping is done interactively, by comparing the intraoperative photograph visually with the rendered image, dragging numbered icons from a palette, and dropping them off at the location corresponding to the numbered tags on the photograph. Once the site has been dropped off the computer performs a 3-D "pick" operation in order to determine the closest surface facet to the site. The vasculature and the cortical surface features guide the user in the accurate localization of the language sites. The two orthogonal MR slices shown on the right of the interface, corresponding to the location of the mouse click on the rendered image, can be used to relate features on the rendered image to the original volume data.

Major cortical landmarks such as the sylvian fissure, central sulcus, and the superior, middle, and inferior temporal gyri are clearly visible in the surface rendering shown in Fig. 3. In addition, the major veins can also be seen in conjunction with cortical anatomy. The stimulation sites have been identified by a neurosurgeon using the cortical landmarks and the blood vessels and correlating the intraoperative photograph with the rendered image. Those sites found intraoperatively to be essential for language are shown enclosed in boxes. After the mapping for a patient is complete, the stimulation sites and their corresponding 3-D coordinates in

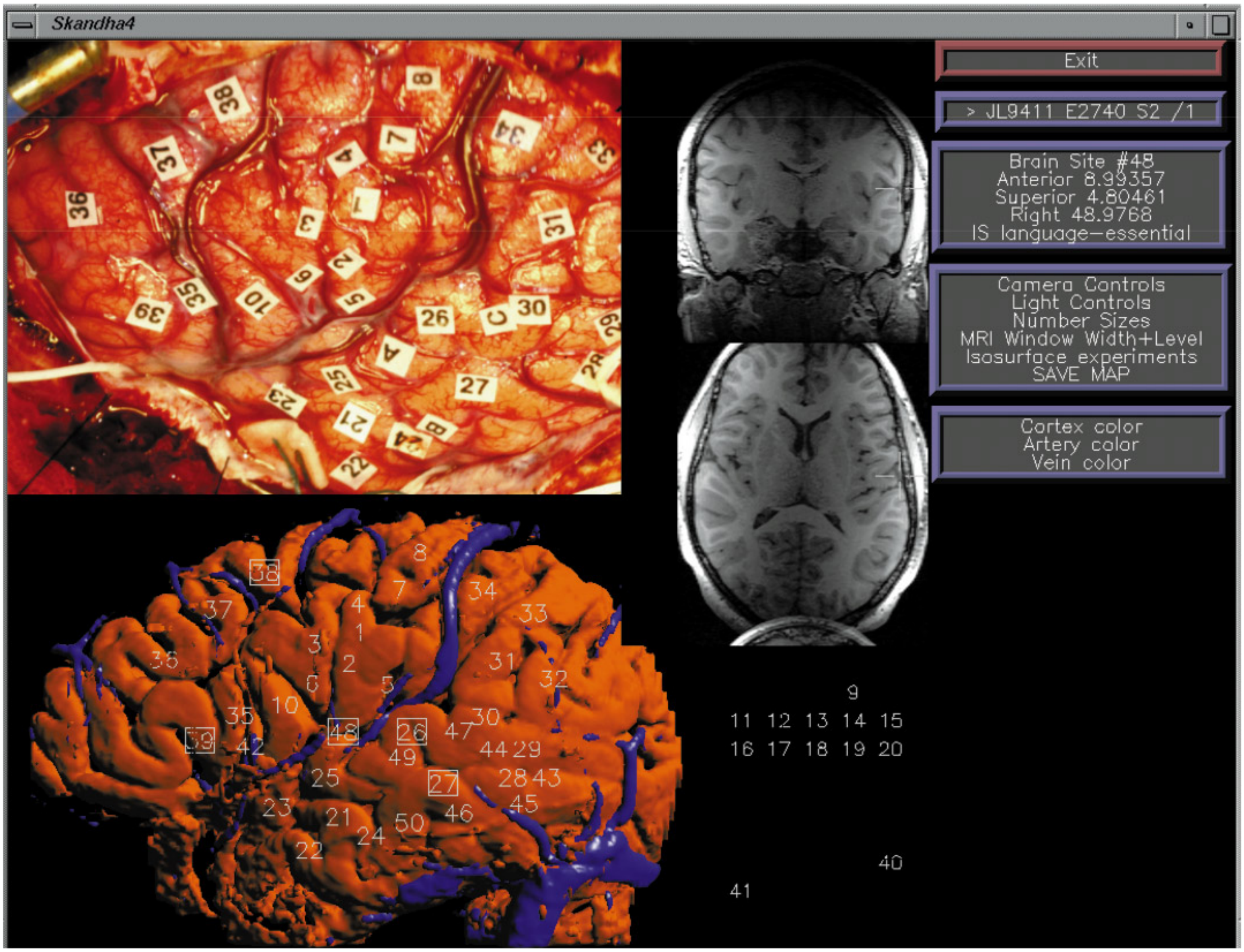

FIG. 3. The interactive brain mapper. Top left of the interface shows the intraoperative photograph. The surface visualization is shown at the bottom left. To the right are MR slices corresponding to the position of the mouse click on the rendered image. The sites, mapped by a neurosurgeon, are shown. Sites marked by small rectangles are essential for language.

MR machine space (based on the surface facet that is found in the pick operation) are stored in a Web-based repository that we are developing for managing multimedia brain map data (Jakobovits *et al.*, 1996).

RESULTS

The visual comparison approach was utilized to map stimulation sites of our first set of 12 patients. All the 311 stimulation sites for the 12 patients were mappable by the neurosurgeon (GO). The mapping results, including sites essential for language, produced by the neurosurgeon, are shown in Figs. 4, 5, and 6 along with the corresponding intraoperative photographs. Note that, as in the earlier study (Ojemann *et al.*, 1989a), there is a high degree of variability in the distribution of language sites.

Repeatability experiments were performed using two groups of mappers—an expert group consisting of a neurosurgeon (GO) and a neuro radiologist (KM) and a nonexpert group consisting of four computer scientists involved in various stages of this project. The mappings were all done independently in a couple of sittings within a week. The time required to map a particular patient depended on the number of stimulation sites and usually varied from 15 to 30 min. Since the intraoperative photo and the rendering did not always have identical aspect and scale, locating landmarks—the initial step employed by all mappers—was time consuming in some cases (e.g., 9602, 9612). Critical cortical landmarks were sometimes not clearly visible because of the poor quality of some intraoperative photographs. In many of the patients, not all the stimulation sites were mapped by all the mappers because the numbered stickers on the sites were not clearly visible to those who were not present at surgery (9410).

For each stimulation site, the mean of the two expert mappings was considered to be the gold standard or the "true" site location. The distances, in three dimensions, of nonexpert mappings from this gold standard were determined. The mean distance of nonexpert mappings from the true stimulation site locations was evaluated for each patient. As mentioned before, not every site was mapped by all the mappers. But for a site to be included in the statistical evaluation, both experts and at least one of the four nonexpert mappers should have mapped it. Table 1 summarizes the results for each patient dataset and the overall mean and standard deviation of the distance of nonexpert mappings from true stimulation site locations. Table 1 also summarizes the variability within the expert group.

A two-mean t test, at 0.05 significance, reveals that the mean distance of nonexpert mappings from the gold standard exceeds the mean distance within the expert group. This suggests a difference between the quality of mappings obtainable by experts and nonexperts, with experts faring slightly better than the nonexperts. However, more experts are needed to verify this conclusion. With a probability of 0.95, the nonexpert mappings fall within a distance of 6.781 mm ($2.87 + 2 \times 1.95$) from the true stimulation site location (4.227 mm for the expert group). Since the language areas and distances between sites are accurate to 1 cm, the accuracies achievable by our method are satisfactory.

We also evaluated the statistics for the various mappings when the experts and nonexperts are not differentiated. The true site locations, instead of being the mean of expert mappings, now become the mean of all the mappings. The results are summarized in Table 2. As can be seen, with a probability of 0.95, the mappings fall within a distance of 5.0717 mm from the true site location.

DISCUSSION

The main contribution of this paper is the demonstration that a visualization-based approach, that takes advantage of human pattern recognition abilities, is adequate for relating invasive surgical stimulation maps to noninvasive imaging modalities. Relatively straightforward image processing algorithms, when applied to high quality MR image datasets, are adequate to produce a rendering of the cortical surface that is close to the appearance of the surface in an intraoperative photograph. Repeatability results show that, given this visualization, accurate mappings can be found even by nonexpert observers, and that the accuracy is well within the accuracy of the stimulation mapping itself. This accuracy is possible using a technique that requires no modification to a long-standing surgical mapping protocol, a nontrivial consideration in a busy clinical environment.

The results provide justification for further pursuit of the visualization-based mapping approach, both to improve the accuracy even further and to use this approach for studying language organization. The results show that, at least for this application, a 3-D position locating device is not required. However, if a locator were needed for other purposes, such as computer-guided surgery, then the mapping procedure would be less labor intensive.

Several factors could contribute to the 5-mm repeatability error when all six observers are combined: (1) user error, (2) the quality of the intraoperative photographs, (3) patient movement during the 50-min acquisition time, and (4) the quality of the segmentation and visualization methods.

We believe that for this study at least, *user error* was not a major factor because each observer was highly motivated to obtain the most accurate mapping results possible, and there was not a large difference between

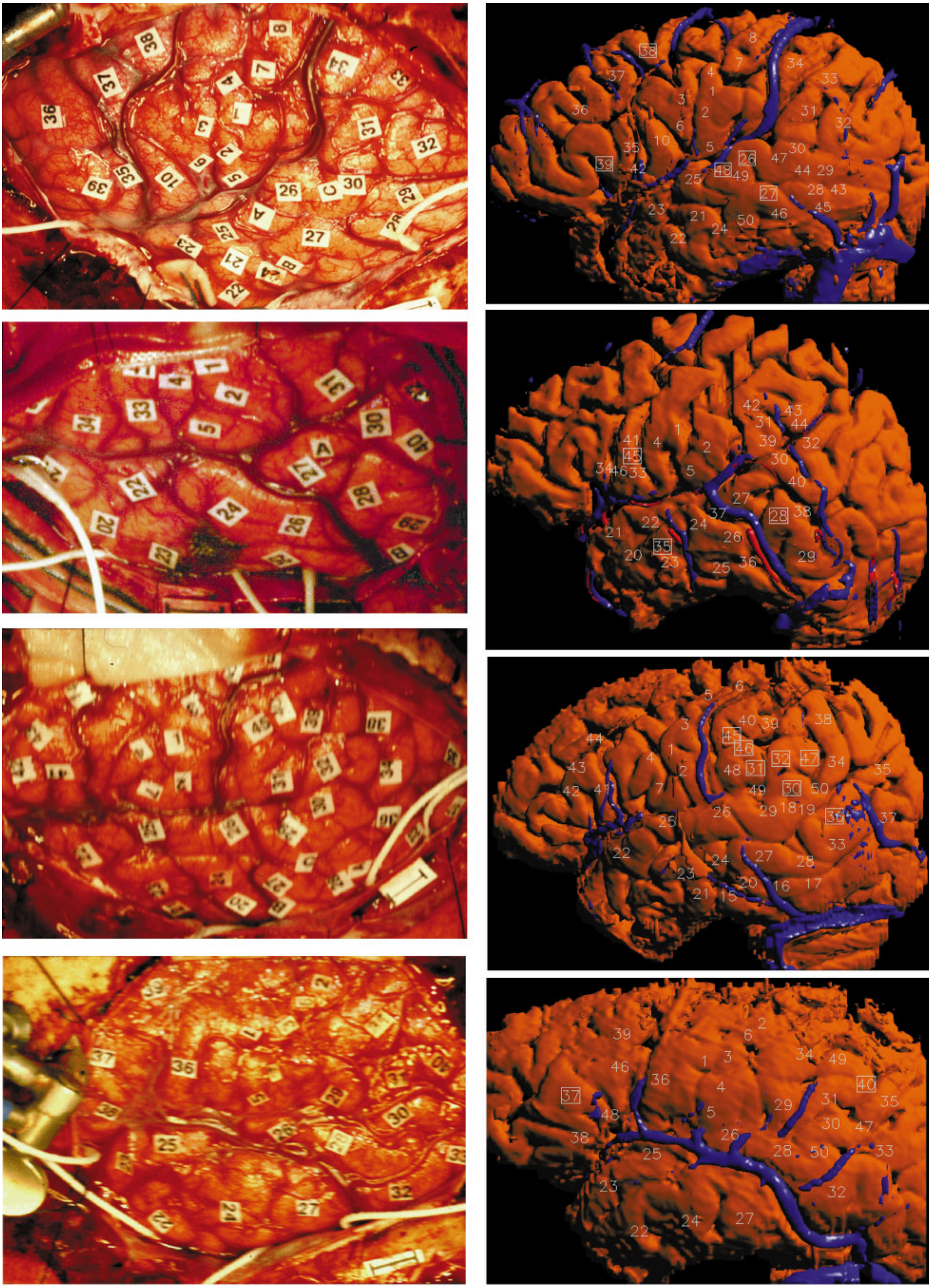

FIG. 4. Mapping results I—Intraop photos and renderings of 9411, 9628, 9415, and 9410. Sites essential for language are marked with rectangles. Additional sites present in the stimulation study, but not in the photograph, have also been mapped. Note that the photographs and the corresponding renderings have different aspects.

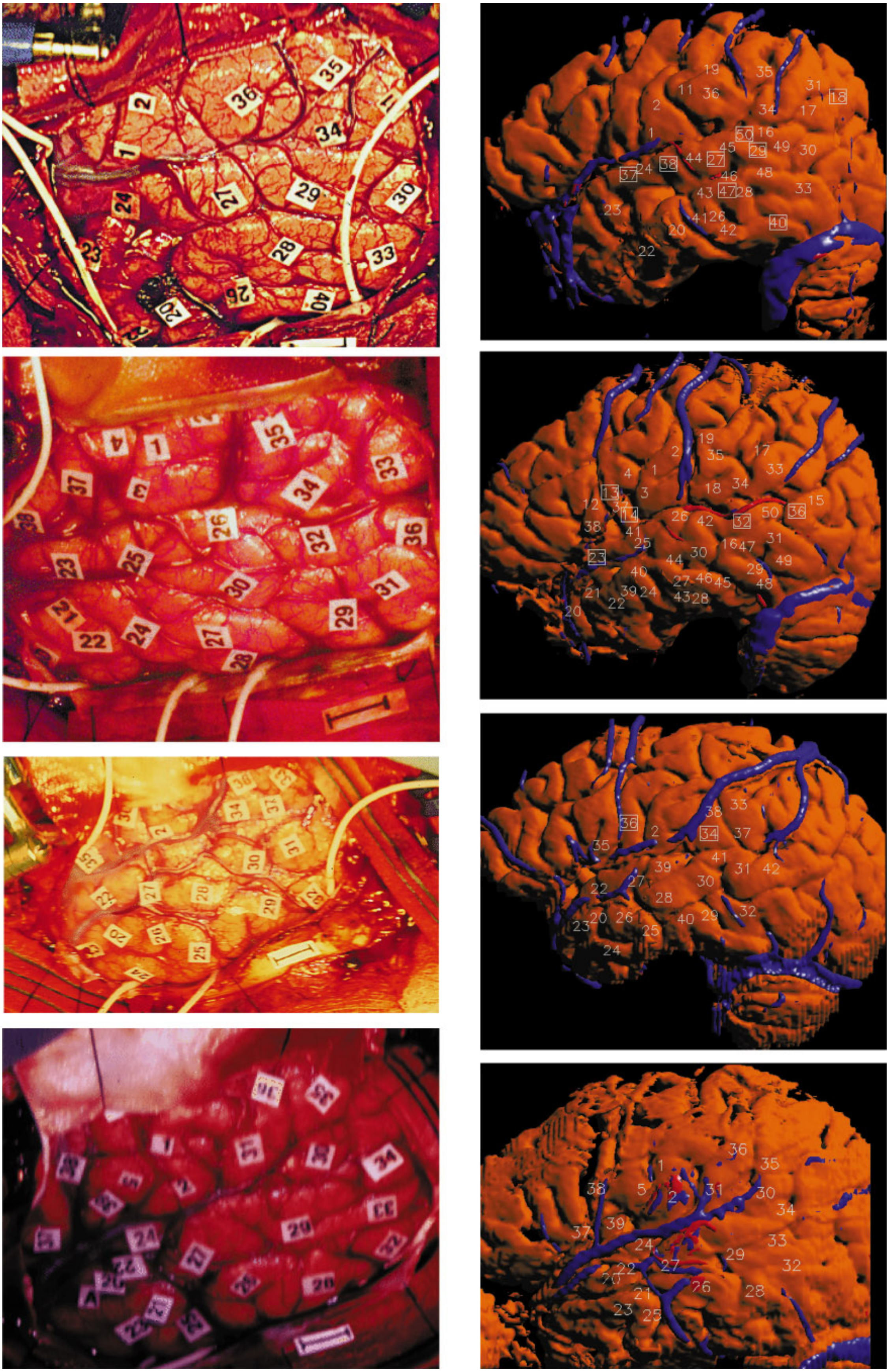

FIG. 5. Mapping results II—Intraop photos and renderings of 9538, 9627, 9612, and 9451.

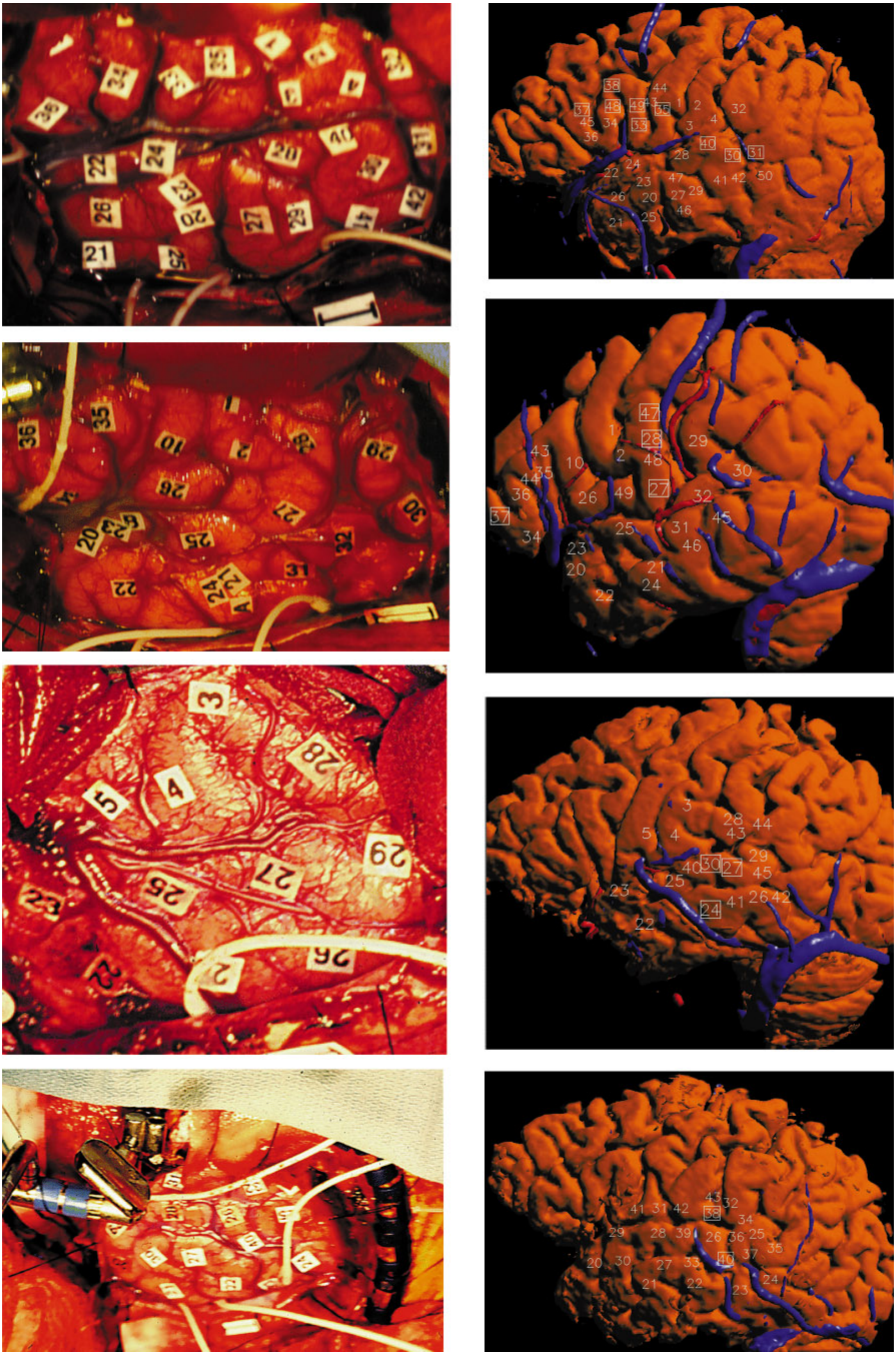

FIG. 6. Mapping results III—Intraop photos and renderings of 9535, 9602, 9618, and 9617.

the experts and nonexperts. However, if this technique were ever to be applied on a more routine basis then user error could become a factor, and the use of a locating device would be more justified.

The *intraoperative photographs* are routinely taken as part of every surgery, using a relatively old camera. If this technique becomes more commonly used then a simple replacement of the camera with a newer digital camera could greatly improve the quality of the photographs.

Potentially the largest source of error is *patient movement* during the 50-min image acquisition time. We believe that for this study this error was not a large factor because (1) the patients were highly motivated to remain still, (2) the patient's head was immobilized with stiff sponges wedged between the head and the sides of the bird-cage head coil, and (3) the arteries and veins were used during mapping only to find the most likely gyrus or sulcus. Once the general area was found the sites were mapped by looking for corresponding sulcal patterns. In fact at least one of the observers turned off the vessel display for the detailed mapping.

Future versions of the visualization system could take advantage of methods that have been developed elsewhere for alignment of different image modalities. For example, the *register* program (Montreal Neurological Institute, 1996) requires the operator to indicate three or more corresponding landmarks between different image datasets, after which the best-fit linear or nonlinear transform is determined such that the residual error between the landmarks is minimized. We used *register* on several of our datasets, but saw no appreciable difference from the original aligned data.

TABLE 1

Repeatability Results

Patient	$d_{\text{nonexpert}}/\sigma_{\text{nonexpert}}$	No. of Mappings	$d_{\text{expert}}/\sigma_{\text{expert}}$	No. of Mappings
9411	2.203/1.360	108	1.484/1.230	54
9415	3.041/2.405	124	1.787/1.439	64
9410	2.717/1.746	71	1.617/1.005	36
9535	2.588/1.430	96	1.429/1.101	48
5988	3.074/1.926	80	2.331/1.718	40
5919	2.821/1.983	84	1.645/1.168	42
9538	2.721/2.142	67	1.277/1.349	34
9602	2.709/1.799	72	1.535/0.679	36
9612	3.185/2.654	75	1.622/1.117	38
9617	3.806/2.273	48	2.509/2.042	26
9618	3.546/2.064	43	1.742/1.134	22
All Patients	2.870/1.955	868	1.699/1.264	440

Note. For a site to be included in the results, both the experts and at least one nonexpert should have mapped it. The second column shows the average distance and standard deviation of a nonexpert mapping from the "true" site location. The fourth column shows the average distance of the expert mappings from the "true" site location. In the absence of a gold standard, the "true" site location is defined as the mean of the expert mappings. All measurements are in mm.

TABLE 2

Overall Repeatability Results

Patient	$d_{\text{mappings}}/\sigma_{\text{mappings}}$	No. of Mappings
9411	1.752/1.257	162
9415	2.143/1.783	188
9410	2.000/1.254	107
9535	1.861/1.085	144
5988	2.092/1.665	120
5919	2.024/1.449	126
9538	1.897/1.572	101
9602	2.026/1.154	108
9612	2.435/1.831	113
9617	2.613/2.014	74
9618	2.503/1.643	65
All Patients	2.077/1.497	1308

Note. The second column shows the average distance of the expert and nonexpert mappings from the "true" site location. If we define the mean of all mappings—expert and nonexpert—to be the "true" site location, the average distance of a mapping is 2.07 mm, with a standard deviation of 1.49 mm.

More recent approaches automate this process by correlating image intensities in the different image datasets (Collins *et al.*, 1994). These techniques have the advantage that they do not require any operator intervention.

The other potential source of error is the quality of the *segmentation and visualization*. Although the region grower and isosurface extraction routines appear to generate very good surfaces, they do not adequately extract the detailed sulcal anatomy, and in some cases not all sulci and gyri are found. For this purpose ongoing work using deformable models (Christensen *et al.*, 1996; Thompson and Toga, 1996), that are augmented to find the cortical details, could be very useful.

Even with the current approach the repeatability results show that this technique is accurate enough to be used both for integrating different kinds of data from the same patient and for integrating data from multiple patients. In both cases the key link is the ability to map all forms of data to a 3-D neuroanatomical model obtained from the MR images.

For example, many techniques have been developed to relate noninvasive imaging modalities such as PET or fMRI to MR-based anatomical images (Collins *et al.*, 1994; Levin *et al.*, 1989). Since the visualization-based mapping approach allows us to relate surgical sites to the MR-based anatomy images, these techniques can be used to relate the surgical sites to PET and fMRI images, among others. If, as suggested by Herholz *et al.* (1997), language maps obtained from noninvasive sources are highly correlated with surgical sites, then it may be possible to altogether supplant intraoperative studies with the more convenient noninvasive methods.

The 3-D neuroanatomical model is also the key to relating data from multiple patients. However, since individual brains are highly variable with respect to even the most common sulci and fissures, it is necessary to normalize the anatomical variations. Although the Talairach coordinate system (Talairach and Tournoux, 1988) is most often used for this purpose, it is not useful for surface mapping because of the highly variable gyral anatomy.

Approaches that may be more relevant for surface mapping include a surface-based coordinate system developed by (Ojemann *et al.*, 1989a), cortical unfolding (Sherk, 1992; Carman *et al.*, 1995; VanEssen and Maunsell, 1980; Jouandet *et al.*, 1989), and deformable models (Christensen *et al.*, 1996; Thompson and Toga, 1996). Although significant challenges remain with each of these techniques, the need for a patient-specific 3-D model is central to all of them.

The development of these and other integration approaches will allow us to further confirm the hypothesis that some but not all of the observed variability in surgical language site distribution can be correlated with anatomic variability. Since it has already been shown that there is a relationship between language site distribution and behavioral measures such as VIQ (Ojemann *et al.*, 1989), it may be possible to demonstrate a relationship between surface anatomy and behavior.

Although such a demonstration will require many more patients, the method described in this paper provides the key to testing these kinds of hypotheses. Since many patient datasets will be needed, an additional requirement is an information management system that can keep track of the large amount of raw and derived image data, as well as stimulation mapping and other clinical data. The system should also allow these data to be related to other language-related information available on the Internet and should provide methods for visualizing the integrated results. We are currently developing such a system as part of the national Human Brain Project (Brinkley *et al.*, 1996; Modayur *et al.*, 1996).

ACKNOWLEDGMENTS

This work was sponsored by Human Brain Project Grant DC/LM02310, cofunded by the National Institute for Deafness and Other Communication Disorders, and the National Library of Medicine. We thank the following individuals for their help in various aspects of this project: Ettore Lettich, Kevin Hinshaw, Rex Jakobovits, and Cornelius Rosse.

REFERENCES

Axel, L., Constantini, J., and Listerud, J. 1987. Intensity correction in surface-coil MR imaging. *Am. J.Radiol.* **148:**418–420.

Binder, J., Rao, S., Hammeke, T., Frost, J., Bandettini, P., Jesmanowicz, A., and Hyde, J. 1995. Lateralized human brain language systems demonstrated by task subtraction functional magnetic resonance imaging. *Arch. Neurol.* **52:**593–601.

Binder, J., Swanson, S., Hammeke, T., Morris, G., Mueller, W., Fischer, M., Benbadis, S., Frost, J., Rao, S., and Haughton, V. 1996. Determination of language dominance using functional MRI: A comparison with WADA test. *Neurology* **46:**978–984.

Brinkley, J., Myers, L., Prothero, J., Heil, G., Tsuruda, J., Maravilla, K., Ojemann, G., and Rosse, C. 1996. A structural information framework for brain mapping. In *Neuroinformatics: An Overview of the Brain Project* (S. H. Koslow and M. F. Huerta, Eds.), pp. 309–334.

Brinkley, J., and Prothero, J. 1997. Slisp: A flexible software toolkit for hybrid, embedded and distributed applications. *Software Pract. Exp.* **27**(1):33–48.

Carman, G., Drury, H., and Van Essen, D. 1995. Computational methods for reconstructing and unfolding the cortex. *Cerebral Cortex* **5**(6):506–517.

Christensen, G., Miller, M., and Vannier, M. 1996. Individualizing neuroanatomical atlases using a massively parallel computer. *IEEE Comp.* **29**(1):32–38.

Collins, D. L., Neelin, P., Peters, T. M., and Evans, A. C. 1994. Automatic 3-D intersubject registration of MR volumetric data in standardized Talairach space. *J. Comp. Assist. Tomogr.* **2:**192–205.

Dawant, B., Zijdenbos, A., and Margolin, R. 1993. Correction of intensity variations in MR images for computer-aided tissue classification. *IEEE Trans. Med. Imaging* **12:**770–781.

Demonet, J., Chollet, F., and Ramsay, S. 1992. The anatomy of phonological and semantic processing in normal subjects. *Brain* **115:**1753–1768.

Elvins, T. 1992. A survey of algorithms for volume visualization. *Comput. Graph.* **26**(3):194–201.

Evans, A. C., Marrett, S., Torrescorzo, J., Ku, S., and Collins, L. 1991. MRI-PET correlation in three dimensions using a volume-of-interest (VOI) atlas. *J. Cerebr. Blood Flow Metab.* **11:**A69–A78.

Haglund, M., Ojemann, G., and Hochman, D. 1992. Optical imaging of epileptiform and functional activity in human cerebral cortex. *Nature* **358:**668–671.

Haglund, M., Berger, M., Shamseldin, M., Lettich, E., and Ojemann, G. 1993. Cortical localization of temporal lobe language sites in patients with gliomas. *Neurosurgery* **34**(4):567–576.

Hayes, C., Tsuruda, J., and Mathis, C. 1993. Temporal lobes: Surface MR coil phased-array imaging. *Radiology* **189**(3):918–920.

Herholz, K., Thiel, A., von Stockhausen, H., Reulen, H., Kessler, J., Ilmberger, J., and Heiss, W. 1997. Presurgical localization of language-related cortex in patients with gliomas of the dominant hemisphere. *Neurology* **48**(3)(Suppl.):A31.

Montreal Neurological Institute, 1996. http://www.mni.mcgill.ca/workshop.html.

Jakobovits, R., Modayur, B., and Brinkley, J. 1996. A Web-based repository manager for brain mapping data. *AMIA Fall Symposium Washington, DC,* 309–313.

Jouandet, M., Tramo, M., Herron, D., Hermann, A., Loftus, W., Bazell, J., and Gazzaniga, M. 1989. Brainprints: Computer-generated two-dimensional maps of the human cerebral cortex in vivo. *J. Cog. Neurosci.* **1:**88–117.

Levin, D., Hu, X., Tan, K., Galhotra, S., Pelizzari, C., Chen, G., Beck, R., Chen, C., Cooper, M., Mullan, J., Hekmatpanah, J., and Spire, J. 1989. The Brain: Integrated three-dimensional display of MR and PET images. *Radiology* **172:**783–789.

Lim, K., and Pfefferbaum, A. 1989. Segmentation of MR brain images in to CSF spaces, white, and gray matter. *J. Cat.* **13**(4):588–593.

Lorensen, W., and Cline, H. 1987. Marching cubes: A high resolution 3-D surface construction algorithm. *Comp. Graph.* **21**(4):163–169.

MacDonald, D., Avis, D., and Evans, A. 1995. Multiple surface identification and matching in magnetic resonance images. *Visual. Biomed. Comp.*

Modayur, B., Prothero, J., Rosse, C., Jakobovits, R., and Brinkley, J. 1996. Visualization and mapping of neurosurgical functional brain data onto a 3-D MR-based model of the brain surface. *AMIA Fall Symposium Washington DC,* 304–308.

Myers, L., and Brinkley, J. 1995. Visualization of brain surface features using registered partially segmented MRI scans. *SPIE Med. Imaging: Image Display,* 43–52.

Ojemann, G., Ojemann, J., Lettich, E., and Berger, M. 1989a. Cortical language localization in left, dominant hemisphere. *J. Neurosurg.* **71:**316–326.

Ojemann, G., Fried, I., and Lettich, E. 1989b. Electrocorticographic (ECOG) correlates of language. I. desynchronization in temporal language cortex during object naming. *EEG Clin. Neurophysiol.* **73:**453–463.

Ojemann, G. 1991. Cortical organization of language and verbal memory based on intraoperative investigations. *Progr. Sensory Physiol.* **12:**193–210.

Petersen, S., Fox, P., Posner, M., Mintun, M., and Raichle, M. 1988. Positron emission tomographic studies of the cortical anatomy of single-word processing. *Nature* **331:**585–589.

Sherk, H. 1992. Flattening the cerebral cortex by computer. *J. Neurosci. Methods* **41**(3):255–267.

Talairach, J., and Tournoux, P. 1988. *Co-planar Stereotaxic Atlas of the Human Brain. 3-Dimensional Proportional System: An Approach to Cerebral Imaging.* Thieme, New York.

Thompson, P., and Toga, A. 1996. A surface-based technique for warping three-dimensional images of the brain. *IEEE Trans. Med. Imaging* **15**(4):402–417.

Van Essen, D., and Maunsell, J. 1980. Two-dimensional maps of the cerebral cortex. *J. Comp. Neurol.* **191:**255–281.